ACS OMEGA

Open Access

http://pubs.acs.org/journal/acsodf

Article

Magnetically Controlled Intraocular Delivery of Dexamethasone Using Silica-Coated Magnetic Nanoparticles

Seungmin Noh, Hye Kyoung Hong, Dong Geun Kim, Hwajun Jeong, Sung Jun Lim, Jin-Young Kim, Se Joon Woo,* and Hongsoo Choi*

Cite This: *ACS Omega* 2024, 9, 27888−27897

Read Online

ACCESS | Metrics & More | Article Recommendations | Supporting Information

ABSTRACT: Although the number of patients with eye diseases is increasing, efficient drug delivery to the posterior segment of the eyeball remains challenging. The reasons include the unique anatomy of the eyeball, the blood−aqueous barrier, the blood−retina barrier, and drug elimination via the anterior chamber and uveoscleral routes. Solutions to these obstacles for therapeutic delivery to the posterior segment will increase the efficacy, efficiency, and safety of ophthalmic treatment. Micro/nanorobots are promising tools to deliver therapeutics to the retina under the direction of an external magnetic field. Although many groups have evaluated potential uses of micro/nanorobots in retinal treatment, most experiments have been performed under idealized in vitro laboratory conditions and thus do not fully demonstrate the clinical feasibility of this approach. This study examined the use of magnetic nanoparticles (MNPs) to deliver dexamethasone, a drug widely used in retinal disease treatment. The MNPs allowed sustainable drug release and successful magnetic manipulation inside bovine vitreous humor and the vitreous humor of living rabbits. Therefore, controlled drug distribution via magnetic manipulation of MNPs is a promising strategy for targeted drug delivery to the retina.

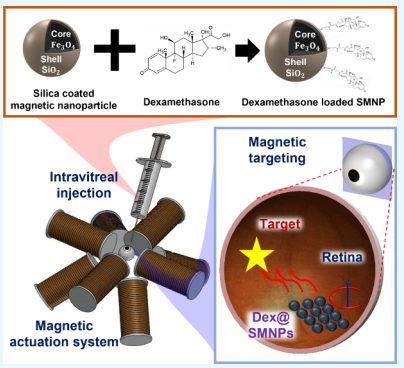

INTRODUCTION

The treatment of ophthalmic diseases varies depending on the type of disease and the affected area. Ointments, topical eye drops, and surgical treatment can be applied to the anterior segment of the eye, including the cornea and anterior chamber.[1,2] However, multiple significant challenges in drug delivery hinder effective treatments for retinal and choroidal diseases. The unique anatomy of the eyeball interferes with accessibility because most of the surface is covered; drug penetration is limited by the blood−aqueous barrier and blood−retina barrier.[3−5]

Direct intravitreal injection of therapeutics into the vitreous humor has been used to treat retinal diseases such as age-related macular degeneration and diabetic retinopathy.[6] However, because of the short half-life of intravitreal therapeutics, repeated injections longer than 4-week intervals are required for chronic retinal diseases; such injections can be a burden to both patients and physicians. Moreover, potential side effects include hemorrhage, retinal detachment, inflammation, and increased intraocular pressure.[7−9] Intravitreal injection itself also has multiple limitations. First, the therapeutic agent injected into the vitreous humor diffuses throughout the eyeball and is eliminated via the anterior and posterior routes.[10] Second, the distribution, degree of spread, and pharmacokinetics within the vitreous cavity are difficult to predict, because they depend on characteristics of the drug; thus, specific targeting of the lesion is rarely assured.[11−13] Third, the concentration of the injected therapeutic agent may decrease by >50% per day, such that <1% of the initial amount remains after 1 week.[14−16] Finally, although implantation-type therapeutics have been introduced for continuous drug release, there is a need to consider the requirement for invasive surgery during implantation and the risk of migration within the vitreous humor, which could block the patient's field of vision.[17−20] Therefore, novel methods for the continuous, effective, and precise delivery of drugs to the target environment are needed.

More effective treatment of posterior eye diseases may be achieved by systems using micro/nanorobots, in which cells or drugs carried on micro/nanosized structures and particles reach the target lesion or release their therapeutic payload close to the target area using a magnetic field.[21−28] The use of nanomilli robots in retinal disease treatment has been explored in multiple studies.[29−33] George et al.[30] demonstrated the feasibility of a method in which a magnetic robot equipped with a needle is used to puncture a retinal vein for retinal disease treatment. However, the robot size was ∼3 mm,

Received: September 14, 2023
Revised: May 26, 2024
Accepted: June 7, 2024
Published: June 20, 2024

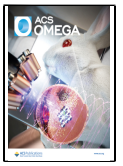

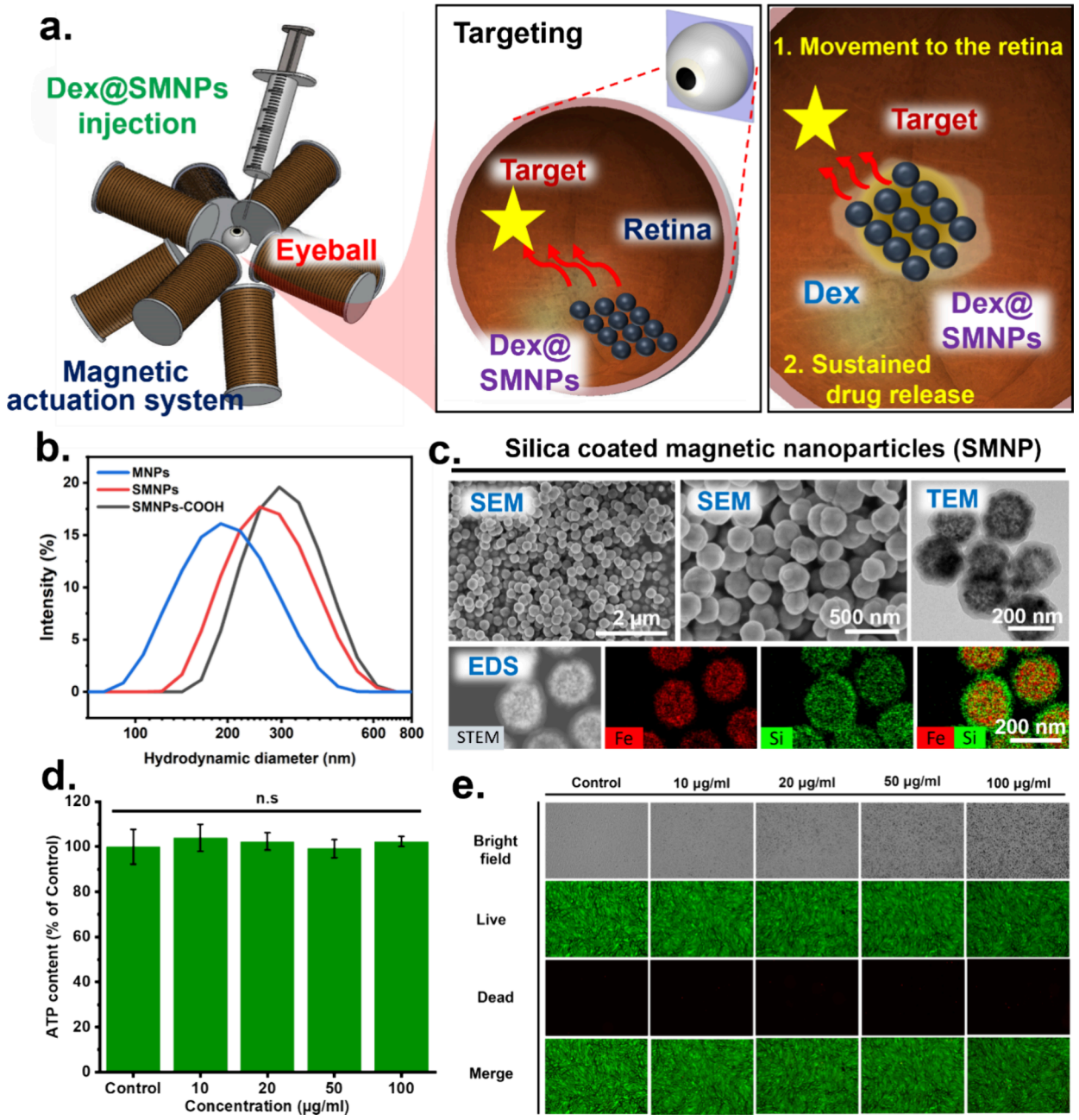

Figure 1. Intraocular drug delivery strategy and fundamental characterization of silica-coated magnetic nanoparticles (MNPs). (a) Schematic images showing drug delivery strategy used in this study (not to scale). (b) Dynamic light scattering data showing the size distribution of particles at each step. SMNPs, silica-coated magnetic nanoparticles; SMNPs-COOH, carboxylic acid-functionalized silica-coated MNPs. (c) Scanning electron microscopy (SEM) and transmission electron microscopy (TEM) micrographs of silica-coated magnetic nanoparticles. (d, e) Biocompatibility of SMNPs determined from ATP content and LIVE/DEAD images, respectively. $*p < 0.05$; ns, not significant. $n = 4$.

sufficiently large to block the patient's field of vision. Moreover, needle-induced rupture of retinal vessels, leading to vitreous hemorrhage, could not be ruled out. Because nickel is not a biocompatible material,[34,35] retrieval of the nickel-based microrobot is required after treatment. These limitations hinder the use of this system in clinical practice. Another study introduced an intraocular microrobot with a microsized helical structure that allowed passage through the mesh-like environment of collagen fibrils, such that the posterior segment could be approached with minimal damage.[31] The perfluorocarbon coating of the microrobot prevented interactions between the microrobot and the vitreous fiber microenvironment. However, both the perfluorocarbon surface coating and the use of nickel to achieve a high level of magnetization limit the utility of this system for clinical drug delivery. Recently, Jiangfan et al.[32] demonstrated swarm control of magnetic nanoparticles (MNPs) inside the vitreous humor using a rotating magnetic field generated by an electromagnetic coil system. The nanoparticles were made hydrophobic via surface treatment with trichloro(1H,1H,2H,2H-perfluorooctyl)silane, which facilitated manipulation in the high-viscosity intraocular environment. These studies demonstrate the potential offered by magnetic manipulation of micro/nanorobots inside the vitreous humor.

https://doi.org/10.1021/acsomega.3c07033
ACS Omega 2024, 9, 27888−27897

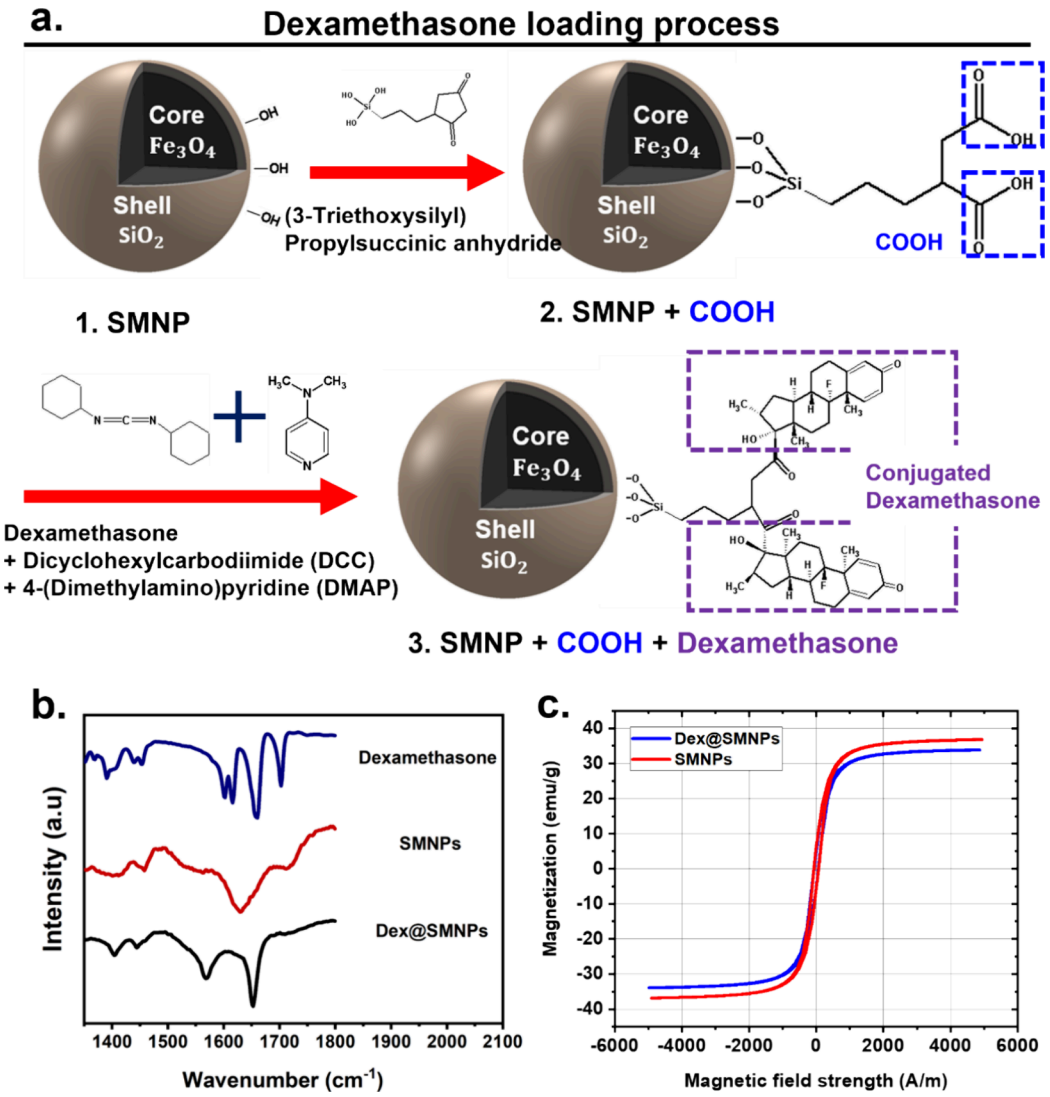

Figure 2. Dexamethasone loading on SMNPs. (a) Stepwise dexamethasone loading on SMNPs. (b) Confirmation of dexamethasone loading by Fourier-transform infrared spectroscopy. (c) Vibrating sample magnetometry data before and after dexamethasone loading.

The most widely used passive-release mechanism for drug-loaded microrobots is diffusion, which requires contact between the drug-loaded surface and the surrounding environment. However, diffusion is difficult if the outermost surface of the robot is a chemical (rather than a drug) that reduces the interaction of the microrobot with the environment to allow better manipulation. Therefore, in the absence of a specific release mechanism, chemically coated microrobots cannot be readily used as passive-release systems. Consequently, the magnetic manipulation of surface-treated micro/nanorobots guarantees operation only in an ideal environment because the release of a therapeutic agent at the target cannot be guaranteed. A more promising approach is one in which, rather than modification for better control, the outermost surface is coated with a drug. However, the manipulation of these particles to achieve drug delivery in the eyeball without surface treatment requires a full understanding of the drug release characteristics of MNPs.

In this study, magnetically controllable dexamethasone-loaded silica-coated MNPs (Dex@SMNPs) were generated for use in the treatment of posterior eye diseases. The silica coating ensured the stable bonding of functional groups and the biocompatibility of the particles; functionalization with carboxylic acid allowed covalent bonding with dexamethasone, a widely used anti-inflammatory drug. Drug release from the particles was demonstrated through incubation with leukemia cells (RS4;11), which are sensitive to dexamethasone. To evaluate the feasibility of magnetic manipulation of the Dex@SMNPs within the vitreous humor, the particles were injected into bovine vitreous humor separated from the eyeball, as well as the vitreous humor of living rabbits. Under a rotating magnetic field generated by a system with eight electromagnetic coils, the particle swarm was sufficiently large to be visible on a camera. Manipulation of the swarm was achieved by tilting the axis of rotation of the magnetic field. These studies demonstrated the feasibility of the magnetic manipulation of Dex@SMNPs in vivo and ex vivo, using materials that can be readily applied in the treatment of posterior eye disease.

RESULTS AND DISCUSSION

Intraocular Drug Delivery Using MNPs. The strategy for intraocular drug delivery using MNPs is described in Figure 1a. To generate required magnetic field, eight-electromagnetic coil system was used. The workspace of the system was a spherical

https://doi.org/10.1021/acsomega.3c07033
ACS Omega 2024, 9, 27888−27897

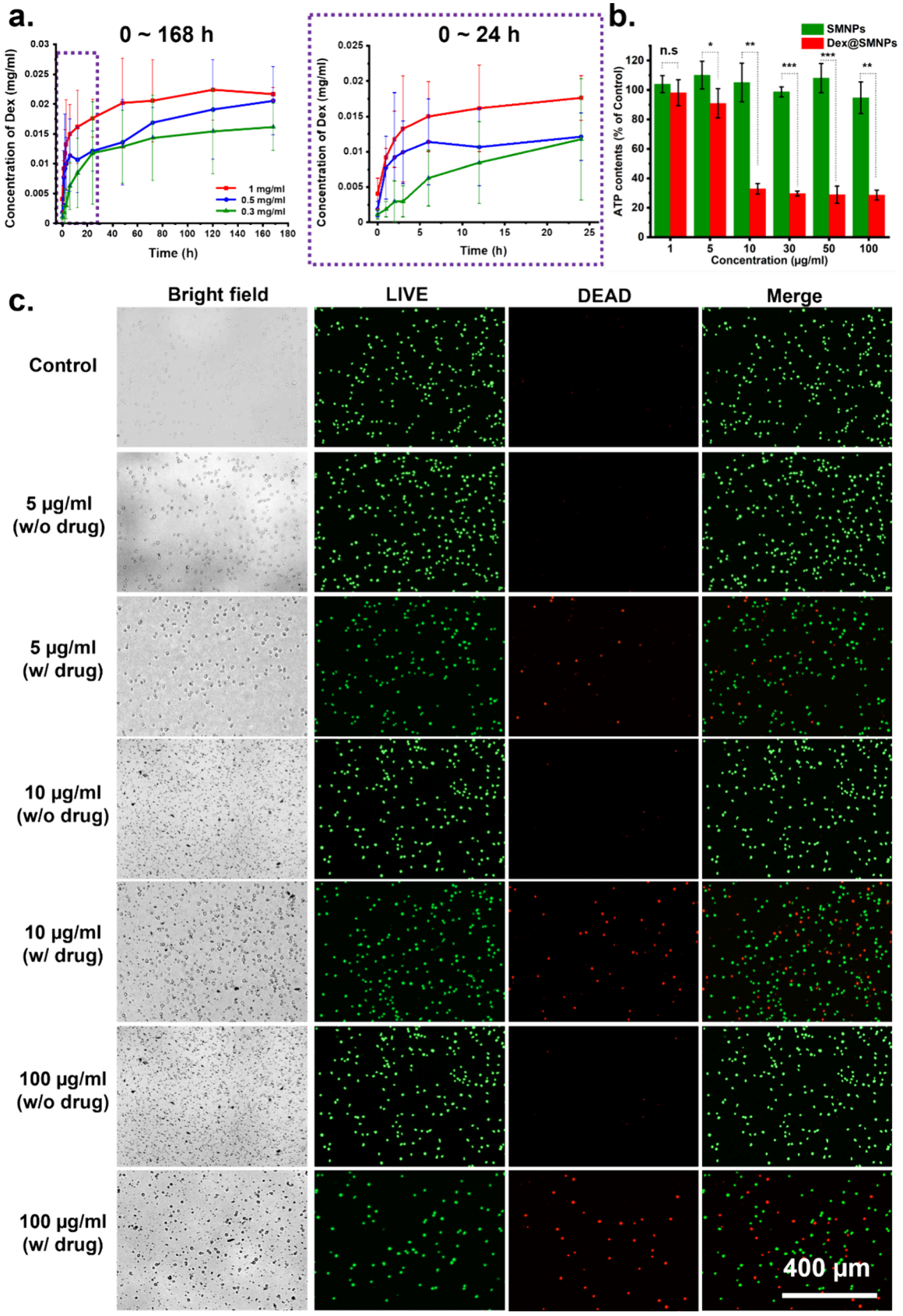

Figure 3. Release of dexamethasone from Dex@SMNPs. (a) Concentration of dexamethasone released from Dex@SMNPs dispersed in PBS (n = 3). (b) Viability of cells cocultured with SMNPs and Dex@SMNPs for 24 h, determined by measuring ATP content. *, $p < 0.05$; **, $p < 0.01$; ***, $p < 0.001$; ns, not significant; n = 4. (c) LIVE/DEAD cell images of cells cocultured with Dex@SMNP for 24 h.

https://doi.org/10.1021/acsomega.3c07033
ACS Omega 2024, 9, 27888−27897

with an approximate diameter of 25 mm, which is large enough to test various eyeballs from different animals (porcine and bovine) (Figure S1). This system also could generate enough magnetic field to make swarm (40 mT) to maintain the swarm. The magnetic field generated by the eight-electromagnetic coil system induced dipole interactions among injected MNPs inside the vitreous humor, causing them to form a chain structure.[36−38] Thanks to the formation of a chain structure, the magnetic nanoparticles could show collective behavior, improving its delivery efficiency. Otherwise, nanovesicles driven by other energy sources are readily scattered because of nondirectionality, such that targeted delivery is not possible.[39−41] In contrast, magnetically actuated carriers have a greater likelihood of following the magnetic field; they can also be more carefully controlled and directed. The swarm of MNPs can be manipulated by changing the orientation of the rotating magnetic field, thus allowing delivery near the target lesion. Swarm formation of the MNPs also reduces the losses that can occur during transportation, resulting in improved therapeutic efficacy related to the larger number of particles reaching the target. Delivery of drug-loaded MNPs near the lesion area enables the maintenance of a higher local drug concentration than is possible with conventional drug injection methods.

Biocompatibility of SMNPs. In this study, SMNPs were used for stable functionalization and biocompatibility of silica.[42−46] The biocompatibility of the SMNPs was verified in previous studies, and their fabrication was performed as previously reported (see Supporting Information). The nanoparticles were then investigated by direct laser spectroscopy (Zetasizer Nano ZS; Malvern Panalytical, Malvern, UK), which revealed a uniform size distribution and a final hydrodynamic diameter (including their carboxylic acid-functionalized silica shell) of ∼300 nm in PBS (Figure 1b). Successful formation of the silica shell was confirmed by scanning electron microscopy, transmission electron microscopy (TEM), and energy-dispersive spectroscopy. As shown in Figure 1c, the SMNPs had a uniform size of ∼200 nm on the TEM image; the core−shell structure (core: Fe_3O_4; shell: silica) could be observed as a cluster of small particles by transmission electron microscopy and energy-dispersive spectroscopy (Figures S2 and S3). In order to manipulate the particles using a magnetic field, the particle size should be large enough and the particle should have superparamagnetic characteristics. However, as the size of the magnetic nanoparticle increases, it loses superparamagnetic characteristics. From this perspective, the particle should be a cluster, small particles aggregated to form one large particles. The core magnetic nanoparticle imparts magnetism to the final particles, allowing the SMNPs to be manipulated in response to an external magnetic field generated by the electromagnetic coil system. The external silica shell guarantees the stable binding of functional groups, as well as biocompatibility. Scanning electron microscopy revealed that the sizes of most SMNPs were 200 nm. To demonstrate their biocompatibility, the SMNPs were cocultured at various concentrations (10, 20, 50, and 100 μg/mL) with the spontaneously arising retinal pigment epithelial cell line ARPE-19 (CRL-2302; ATCC, Manassas, VA, USA). After 48 h, cell viability was evaluated based on the change in adenosine triphosphate (ATP) content and the results of a LIVE/DEAD assay. As shown in Figure 1d, e, the SMNPs did not exhibit significant cytotoxicity, even at the highest concentration (100 μg/mL). These results confirmed the potential for the use of SMNPs as therapeutic delivery agents.

Dexamethasone Loading on SMNPs. After biocompatibility had been confirmed, SMNPs were electrostatically loaded with dexamethasone, one of the most widely used drugs in ophthalmic treatment,[47−49] in accordance with an established protocol (Figure 2a).[50] Briefly, 12 mg of carboxylic acid-functionalized SMNPs were washed with ethanol and dichloromethane (DCM; 270997, Sigma-Aldrich, St. Louis, MO, USA). The SMNPs were then dispersed in 1.92 mL of DCM containing 21 mg of N,N′-dicyclohexylcarbodiimide (DCC; D80002; Sigma-Aldrich) and 5 mg of 4-(dimethylamino)pyridine (DMAP; 107700; Sigma-Aldrich). After 20 min of incubation, 5.6 mg of dexamethasone was added, and the solution was mixed for 3 days using a magnetic stirring bar. Finally, the dexamethasone-loaded SMNPs (Dex@SMNPs) were washed with ethanol and lyophilized until further use. Both the functional group on the silica shell and dexamethasone loading were examined using Fourier-transform infrared spectroscopy. As shown in Figure 2b, the characteristic peak of dexamethasone was detected at 1,660 cm^{-1}; a Dex@SMNP peak at 1,652 cm^{-1} indicated successful conjugation of the drug to the SMNPs. Because of the paramagnetic characteristics of the MNPs, both the SMNPs and the Dex@SMNPs also showed paramagnetism, with maximum values of 37 and 34 emu/g, respectively (Figure 2c). The weight ratio of the MNPs was reduced as additional materials were added, leading to a slightly reduced maximum magnetization value per unit weight. Importantly, the silica used to coat the MNPs is biocompatible and can be treated with stable and diverse functional groups; therefore, it can presumably be used to support other types of drugs in clinical applications.

Dexamethasone Release from SMNPs. Dex@SMNPs at concentrations of 0.3, 0.5, and 1 mg/mL were stored in phosphate-buffered saline (PBS; Welgene, Gyeongsan, South Korea) for 7 days to measure dexamethasone release over time. To mimic in vivo release, the samples were placed in an incubator (37 °C, 5% CO_2) and the concentration of released dexamethasone was measured at various time points. At each time point, 3 μL of solution was collected from the vial and replaced with PBS to maintain the total volume. The amount of released dexamethasone was then measured by ultraviolet (UV)-visible spectrometry (Figure S4). As shown in Figure 3a, a large amount of dexamethasone was released in the initial stage (within 24 h) from all three concentrations, and saturation was reached over time.

$$\text{Drug loading efficiency} = \frac{\text{Weight of the drug in SMNPs}}{\text{Weight of the feeding drug}} \quad (1)$$

By day 7, 6.48 ± 0.33, 6.17 ± 1.73, and 4.85 ± 1.19 μg of dexamethasone had been released from 300-μL amounts of Dex@SMNPs suspensions at 1, 0.5, and 0.3 mg/mL respectively. The drug loading efficiency was calculated with the aid of eq 1. Assuming complete drug release from Dex@SMNPs loaded at a drug level of 0.3 mg/mL, the loading efficiency was at least 8.7%. The cytotoxicity of the released dexamethasone was examined by coculturing the Dex@SMNPs with leukemia cells for 48 h; although leukemia was not the target disease model in this study, these cells were used because of their sensitivity to dexamethasone.[51,52] Whereas no significant cytotoxicity was observed in cells cultured with any

https://doi.org/10.1021/acsomega.3c07033
ACS Omega 2024, 9, 27888−27897

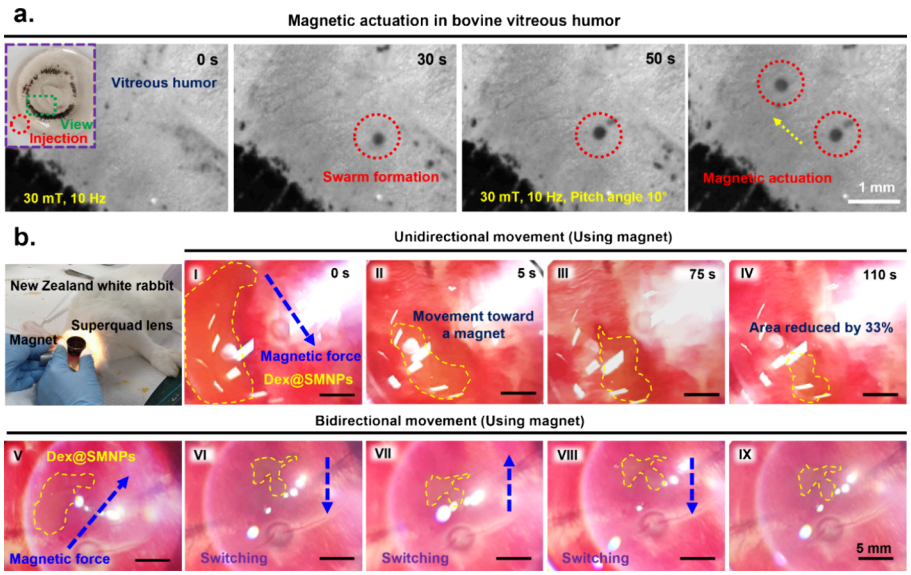

Figure 4. Magnetic manipulation of Dex@SMNPs within vitreous humor. (a) Magnetic actuation in vitreous humor of bovine eyes obtained within 2 days after slaughter (ex vivo). (b) Magnetic attraction of Dex@SMNPs inside vitreous humor of living New Zealand white rabbits (in vivo) under unidirectional and bidirectional movement conditions.

concentration of SMNPs alone (Figure 3b, c), concentration-dependent cytotoxic effects were observed in cells cultured with Dex@SMNPs (Figure 3b, c and Figure S5). At concentrations >10 μg/mL, the ATP content of the cocultured cells sharply decreased compared to 5 μg/mL group. Because the leukemia cells were cultured in suspension form, the culture plates were centrifuged for 30 s prior to visualization by fluorescence microscopy. As shown in Figure 3c, the LIVE/DEAD fluorescence images after 24 h of coculture were consistent with the ATP data. No stimulus was required for complete release of covalently bound dexamethasone; the release rate was sufficiently slow to ensure that all Dex@SMNPs attained the target lesion. Not all dexamethasone was released before the target was reached. After the Dex@SMNPs became located in diseased regions, they continuously released drug without the need for any stimulation. These experiments demonstrated the potential for MNPs to be used in targeted delivery and the release of therapeutic agents to the retina or posterior segment of the eye.

Magnetic Manipulation of Dex@MNPs Inside the Vitreous Humor. The magnetic manipulation of Dex@SMNPs in bovine vitreous humor was then studied. To minimize protein degeneration, bovine eyeballs obtained within 2 days of slaughter were used in the experiment. The vitreous humor was separated from the bovine eyeball and placed on a plate with the pupil oriented upward; 20 μL of Dex@SMNPs (concentration of 1 mg/mL, dispersed in PBS) were injected into the underside of the vitreous humor using a 26-gauge syringe needle, thus mimicking intravitreal injection in the clinical setting (Figure 4a). There were no difficulties during intravitreal injection, such as needle blockage by the particles. The Dex@SMNP-injected vitreous humor was then placed on the workspace of the magnetic actuation system, which included a charge-coupled device (CCD) camera for magnetic actuation and imaging. Immediately after injection, the 200 nm Dex@SMNPs were evenly spread, but individual particles could not be imaged with the CCD camera. A rotating magnetic field (30 mT, 10 Hz) was applied until a swarm of particles was generated (~30 s) (Figure 4a and Video 1). A low rotating frequency cannot form a swarm, and a high rotating frequency that is too high forms multiple swarms at once, which can induce the loss of MNPs during the manipulation. Therefore, the optimized magnetic field (30 mT, 10 Hz) was applied after several attempts. After 50 s, the swarm had stabilized. When the axis of the rotational magnetic field was altered (i.e., the pitch angle was changed to 10°), the particles began to move to the upper left. The speed of the swarm was ~149 μm/s, which was sufficiently fast to reach the target before complete release of the therapeutic agent. This experiment demonstrated the successful intraocular manipulation of particles without any surface treatment, which reduced interactions between the particles and vitreous humor.

Animal Experiment. An in vivo experiment was performed in 3-week-old New Zealand white rabbits because the vitreous body viscosity is similar in rabbits and humans.[53] Dex@SMNPs dispersed in PBS (1 mg/mL), at the same concentrations as in the ex vivo experiment, were injected through the pars plana in the superotemporal quadrant using a 26-gauge needle. The intraocular particles were observed using a widefield contact lens (Super Quad 160, Volk Optical). After intravitreal injection, the Dex@SMNPs formed a broad layer (yellow dotted line in Figure 4b-I). To gather the diffuse nanoparticles within a single location, a 300-mT magnet was placed over the superior portion of the rabbit eyeball. The blue arrows indicate the directions in which the magnetic forces moved the dispersed Dex@SMNPs and yellow dotted circle indicate the occupied area by the injected Dex@SMNPs. Because of the high strength of the magnet, the Dex@SMNPs readily aggregated. Magnetic attraction was evaluated through examination of the area occupied by the particles using ImageJ (National Institutes of Health, Bethesda, MD, USA). Table S1 shows the area of Dex@SMNP distribution inside the vitreous humor. Five seconds after the magnet had been placed on the rabbit eyeball, the Dex@SMNPs moved toward the vitreous cortex (near the magnet; Figure 4b), such that the area of vitreous humor occupied by nanoparticles was reduced to 40% compared with the initial state (Figure 4b-II). Subsequently, movement of the Dex@SMNPs became significantly slower.

https://doi.org/10.1021/acsomega.3c07033
ACS Omega 2024, 9, 27888−27897

After 75 s (Figure 4b-III), the particles were denser than in the initial state, occupying 33% of the area. After 110 s (Figure 4b-IV), the area of nanoparticles had decreased to approximately 18% compared with the initial state, indicating successful targeting of the retina by the external magnetic field. In the second experiment, the location of the magnet was changed at 2-s intervals to evaluate the bidirectional movement of the injected Dex@SMNPs. As shown in Figure 4b-V−IX, the occupied area was only reduced to ∼40% because the Dex@SMNPs lacked sufficient time to aggregate; their location changed according to the magnetic field. Magnetic manipulation-based targeting of the SMNPs to the posterior segment of the eyeball could facilitate the local efficient release of their drug cargo in the target area. In this experiment, only dexamethasone was tested, but other therapeutics (e.g., genes or drugs) could presumably also be used. Furthermore, unlike previous studies with micro/nanorobots, the surface of the Dex@SMNPs was not treated to minimize interactions between the particles and vitreous humor. It was demonstrated that it was possible to manipulate Dex@SMNPs in a high viscosity environment without additional surface treatment. The higher viscosity of the rabbit vitreous humor, compared with the bovine vitreous humor tested ex vivo, led to slower movement of SMNPs. The response of Dex@SMNPs to the gradient magnetic field revealed that MNPs could serve as platforms for controlled delivery of ophthalmic drugs. Such delivery is not possible via conventional intravitreal injection.

CONCLUSIONS

In previous studies, micro/nanorobots tested as drug delivery systems for eye diseases were surface tailored to maximize control inside the vitreous humor, but their perfluorocarbon or silane surface coatings lacked biocompatibility, which prevented clinical application. The present study evaluated the use of dexamethasone-loaded SMNPs (Dex@SMNPs) without surface treatment to reduce interactions between the particles and the vitreous humor microenvironment. The SMNPs provided a biocompatible shell and allowed stable functionalization. The covalently bonded dexamethasone was successfully released over 7 days, without any stimulus, under standard cell culture conditions (37 °C, 5% CO_2). The Dex@SMNPs exhibited alignment via dipole interaction; in isolated bovine vitreous humor, they could be controlled by an external magnetic field. Application of the magnetic field from outside the eyeball successfully moved the Dex@SMNPs to an area close to the target within the eyeball. Thus, magnetized intravitreally injected drug-loaded MNPs can be used to increase the concentration of drug delivered to the target site. Because the MNPs were successfully manipulated even in highly viscous fluids, such as vitreous humor, drug-loaded MNPs are expected to be useful in most fluid-filled areas of the body. Overall, the MNP-mediated delivery of therapeutics, which overcomes the limitations of low drug concentration and poor targeting ability, could replace conventional treatments in many settings.

METHODS

Dexamethasone Loading on SMNPs. Dexamethasone loading was conducted using a previously published protocol.[50] First, 12 mg of MNPs washed with ethanol were placed in a vial with 21 mg of DCC (D80002; Sigma-Aldrich) and 5 mg of DMAP (107700; Sigma-Aldrich). After the addition of 1.92 mL of DCM (270997; Sigma-Aldrich), the samples were rotated at room temperature for 20 min. DCM was added at the final step because it rapidly evaporates under normal conditions. Dexamethasone (5.6 mg) was then added, and the solution was mixed for 3 days with a magnetic stirring bar. The dexamethasone-loaded MNPs were separated, washed with ethanol triplicate, lyophilized, and stored in capped vials until use.

Magnetic Manipulation of SMNPs. Magnetic manipulation of SMNPs was evaluated using bovine vitreous humor (Biozoa, Gyeonggi-do, Korea). Bovine eyes obtained within 2 days of slaughter were used to minimize protein denaturation. Vitreous humor was separated from the eyeballs and placed on a plate in the working space of the magnetic actuation system. Lyophilized Dex@SMNPs were dispersed in PBS at a concentration of 1 mg/mL, then sonicated to achieve an even distribution. A syringe with a 30-gauge needle was filled with the prepared suspension, and ∼100 μL of Dex@SMNPs were injected into the bovine vitreous humor. A swarm of injected Dex@SMNPs was created by applying a rotating magnetic field (30 mT, 10 Hz). After swarm formation, the rotating magnetic field was tilted 10° to manipulate the swarm.

Animal Experiment. The animal experiment protocol was approved by the Animal Experiment Ethics Committee of DGIST (approval number: DGIST-IACUC-22042601−0004). New Zealand white rabbits were anesthetized by intramuscular injection of a mixture of Zoletil and xylazine (0.5 μL/g and 0.2 μL/g, respectively). The eye was then anesthetized with a drop of 0.5% proparacaine hydrochloride. Dex@SMNPs suspended in PBS were intravitreally injected in a volume of 30 μL outside the iris, as in an actual clinical procedure. A magnet with a maximum intensity of 300 mT was placed on the top of the rabbit's head to localize the Dex@SMNPs near the retina. Rabbit fundus images were obtained using a super quad lens, and images of SMNPs in the eyeball were obtained using a CCD camera. The area occupied by SMNPs was quantified using ImageJ software (National Institutes of Health).

Statistical Analysis. All data are presented as means ± standard deviations of at least three independent experiments or samples. All statistical analyses were performed using Microsoft Excel (Microsoft Corp., Redmond, WA, USA) and two-sample t tests, assuming inhomogeneity of variance. In all analyses, p-values <0.05 were considered indicative of statistical significance.

ASSOCIATED CONTENT

Supporting Information

The Supporting Information is available free of charge at https://pubs.acs.org/doi/10.1021/acsomega.3c07033.

Detailed experimental methods and characterization; Eight-electromagnetic coil system (Figure S1); Transmission electron micrographs of magnetic nanoparticles before and after the silica shell coating (Figure S2); Energy-dispersive X-ray spectroscopy spectra of silica-coated magnetic nanoparticles (Figure S3); Calibration plot of UV spectrometer according to dexamethasone concentration (Figure S4); Viability of leukemia cells after incubation with Dex@SMNPs for 24 h (Figure S5); Area occupied by Dex@SMNPs in vitreous humor in vivo (PDF)

Magnetic manipulation of Dex@SMNPs inside the vitreous humor (MP4)

https://doi.org/10.1021/acsomega.3c07033
ACS Omega 2024, 9, 27888−27897

AUTHOR INFORMATION

Corresponding Authors

Se Joon Woo − *Department of Ophthalmology, Seoul National University College of Medicine, Seoul National University Bundang Hospital, Seongnam 13620, Republic of Korea*; Email: sejoon1@snu.ac.kr

Hongsoo Choi − *Department of Robotics and Mechatronics Engineering, Daegu Gyeong-buk Institute of Science and Technology (DGIST), Daegu 42988, Republic of Korea; DGIST-ETH Microrobotics Research Center, DGIST, Daegu 42988, Republic of Korea;* orcid.org/0000-0003-3613-2833; Email: mems@dgist.ac.kr

Authors

Seungmin Noh − *Department of Robotics and Mechatronics Engineering, Daegu Gyeong-buk Institute of Science and Technology (DGIST), Daegu 42988, Republic of Korea; DGIST-ETH Microrobotics Research Center, DGIST, Daegu 42988, Republic of Korea*

Hye Kyoung Hong − *Department of Ophthalmology, Seoul National University College of Medicine, Seoul National University Bundang Hospital, Seongnam 13620, Republic of Korea*

Dong Geun Kim − *Department of Ophthalmology, Inje University College of Medicine, Busan Paik Hospital, Busan 47392, Republic of Korea*

Hwajun Jeong − *Division of Nanotechnology, DGIST, Daegu 42988, Republic of Korea*

Sung Jun Lim − *Division of Nanotechnology, DGIST, Daegu 42988, Republic of Korea;* orcid.org/0000-0002-4504-597X

Jin-Young Kim − *DGIST-ETH Microrobotics Research Center, DGIST, Daegu 42988, Republic of Korea*

Complete contact information is available at: https://pubs.acs.org/10.1021/acsomega.3c07033

Author Contributions

This work was conceptualized by S.N., H.K.H, S.J.W., and H.C. The magnetic nanoparticles were fabricated by H.J. and S.J.L. All the in vitro experiments were conducted by S.N., and the animal experiment was performed by D.G.K. under the supervision of S.J.W. and H.C. The experimental analysis was conducted by H.K.H. and D.G.K. This manuscript was written by S.N. and revised by S.J.W. and H.C.

Funding

The National Convergence Research of Scientific Challenges through the National Research Foundation of Korea (NRF) (2021M3F7A1082275), the DGIST R&D Program (23-CoE-BT-02), the Seoul National University Bundang Hospital (13-2024-0001), and NRF by the Korea government (Ministry of Science and ICT) (RS-2023-00248480).

Notes

The authors declare no competing financial interest.

ACKNOWLEDGMENTS

The author thanks all the members of DGIST-ETH Microrobotics Research Center and Biomicrorobotics Lab for their sincere help and comments.

ABBREVIATIONS

MNP, magnetic nanoparticles; Dex, Dexamethasone; SMNP, silica coated magnetic nanoparticle; Dex@SMNP, dexamethasone loaded silica coated magnetic; DCM, dichloromethane; DCC, *N*,*N*′-dicyclohexylcarbodiimide; DMAP, 4-(dimethylamino)pyridine; TEM, transmission electron microscopy; SEM, scanning electron microscope; ATP, adenosine triphosphate; PBS, phosphate buffer saline

REFERENCES

(1) Messmer, E. M. The pathophysiology, diagnosis, and treatment of dry eye disease. *Dtsch Arztebl Int.* **2015**, *112* (5), 71.

(2) Molokhia, S. A.; Thomas, S. C.; Garff, K. J.; Mandell, K. J.; Wirostko, B. M. Anterior eye segment drug delivery systems: current treatments and future challenges. *J. Ocul. Pharmacol.* **2013**, *29* (2), 92−105.

(3) Cabrera, F. J.; Wang, D. C.; Reddy, K.; Acharya, G.; Shin, C. S. Challenges and opportunities for drug delivery to the posterior of the eye. *Drug Discovery* **2019**, *24* (8), 1679−1684.

(4) Urtti, A. Challenges and obstacles of ocular pharmacokinetics and drug delivery. *Adv. Drug Delivery Rev.* **2006**, *58* (11), 1131−1135.

(5) Cholkar, K.; Dasari, S. R.; Pal, D.; Mitra, A. K. Eye: Anatomy, physiology and barriers to drug delivery. *Ocular transporters and receptors, Ocular Transporters and Receptors* **2013**, 1−36.

(6) Sampat, K. M.; Garg, S. J. Complications of intravitreal injections. *Curr. Opin Ophthalmol.* **2010**, *21* (3), 178−183.

(7) Storey, P. P.; Pancholy, M.; Wibbelsman, T. D.; Obeid, A.; Su, D.; Borkar, D.; Garg, S.; Gupta, O. Rhegmatogenous retinal detachment after intravitreal injection of anti−vascular endothelial growth factor. *Ophthalmology.* **2019**, *126* (10), 1424−1431.

(8) Baek, S. U.; Park, I. W.; Suh, W. Long-term intraocular pressure changes after intravitreal injection of bevacizumab. *Cutan. Ocul. Toxicol.* **2016**, *35* (4), 310−314.

(9) Sato, T.; Emi, K.; Ikeda, T.; Bando, H.; Sato, S.; Morita, S.-i.; Oyagi, T.; Sawada, K. Severe intraocular inflammation after intravitreal injection of bevacizumab. *Ophthalmology.* **2010**, *117* (3), 512−516.

(10) Kim, H. M.; Ha, S.; Hong, H. K.; Hwang, Y.; Kim, P.; Yang, E.; Chung, J. Y.; Park, S.; Park, Y. J.; Park, K. H.; Kim, H.; Woo, S. J. Intraocular distribution and kinetics of intravitreally injected antibodies and nanoparticles in rabbit eyes. *Transl Vis Sci. Technol.* **2020**, *9* (6), 20−20.

(11) Henein, C.; Awwad, S.; Ibeanu, N.; Vlatakis, S.; Brocchini, S.; Tee Khaw, P.; Bouremel, Y. Hydrodynamics of intravitreal injections into liquid vitreous substitutes. *Pharmaceutics.* **2019**, *11* (8), 371.

(12) Velentza-Almpani, A.; Ibeanu, N.; Liu, T.; Redhead, C.; Tee Khaw, P.; Brocchini, S.; Awwad, S.; Bouremel, Y. Effects of flow hydrodynamics and eye movements on intraocular drug clearance. *Phamaceutics.* **2022**, *14* (6), 1267.

(13) Kim, H. M.; Park, K. H.; Chung, J. Y.; Woo, S. J. A prediction model for the intraocular pharmacokinetics of intravitreally injected drugs based on molecular physicochemical properties. *Ophthalmic Res.* **2020**, *63* (1), 41−49.

(14) Zhang, L.; Li, Y.; Zhang, C.; Wang, Y.; Song, C. Pharmacokinetics and tolerance study of intravitreal injection of dexamethasone-loaded nanoparticles in rabbits. *Int. J. Nanomedicine.* **2009**, 175−183.

(15) Gan, I. M.; Ugahary, L. C.; van Dissel, J. T.; van Meurs, J. C.; E. Effect of intravitreal dexamethasone on vitreous vancomycin concentrations in patients with suspected postoperative bacterial endophthalmitis. *Graefes Arch Clin Exp Ophthalmol.* **2005**, *243*, 1186−1189.

(16) Bakri, S. J.; Snyder, M. R.; Reid, J. M.; Pulido, J. S.; Ezzat, M. K.; Singh, R. J. Pharmacokinetics of intravitreal ranibizumab (Lucentis). *Ophthalmology.* **2007**, *114* (12), 2179−2182.

(17) Fassbender Adeniran, J. M.; Jusufbegovic, D.; Schaal, S. Common and rare ocular side-effects of the dexamethasone implant. *Ocul. Immunol. Inflamm.* **2017**, *25* (6), 834−840.

(18) Khurana, R. N.; Appa, S. N.; McCannel, C. A.; Elman, M. J.; Wittenberg, S. E.; Parks, D. J.; Ahmad, S.; Yeh, S. Dexamethasone

implant anterior chamber migration: risk factors, complications, and management strategies. *Ophthalmology.* **2014**, *121* (1), 67−71.
(19) Celik, N.; Khoramnia, R.; Auffarth, G. U.; Sel, S.; Mayer, C. S. Complications of dexamethasone implants: risk factors, prevention, and clinical management. *Int. J. Ophthalmol.* **2020**, *13* (10), 1612.
(20) Lim, J. I.; Wolitz, R. A.; Dowling, A. H.; Bloom, H. R.; Irvine, A. R.; Schwartz, D. M. Visual and anatomic outcomes associated with posterior segment complications after ganciclovir implant procedures in patients with AIDS and cytomegalovirus retinitis. *Am. J. Ophthalmol.* **1999**, *127* (3), 288−293.
(21) Noh, S.; Jeon, S.; Kim, E.; Oh, U.; Park, D.; Park, S. H.; Kim, S. W.; Pané, S.; Nelson, B. J.; Kim, J. y.; Choi, H. A biodegradable magnetic microrobot based on gelatin methacrylate for precise delivery of stem cells with mass production capability. *Small.* **2022**, *18* (25), No. 2107888.
(22) Kim, E.; Jeon, S.; An, H.-K.; Kianpour, M.; Yu, S.-W.; Kim, J.-y.; Rah, J.-C.; Choi, H. A magnetically actuated microrobot for targeted neural cell delivery and selective connection of neural networks. *Sci. Adv.* **2020**, *6* (39), No. eabb5696.
(23) Magdanz, V.; Khalil, I. S.; Simmchen, J.; Furtado, G. P.; Mohanty, S.; Gebauer, J.; Xu, H.; Klingner, A.; Aziz, A.; Medina-Sánchez, M.; Schmidt, O. G.; Misra, S. IRONSperm: Sperm-templated soft magnetic microrobots. *Sci. Adv.* **2020**, *6* (28), No. eaba5855.
(24) Li, J.; Li, X.; Luo, T.; Wang, R.; Liu, C.; Chen, S.; Li, D.; Yue, J.; Cheng, S.-h.; Sun, D. Development of a magnetic microrobot for carrying and delivering targeted cells. *Sci. Robot.* **2018**, *3* (19), No. eaat8829.
(25) Ceylan, H.; Yasa, I. C.; Yasa, O.; Tabak, A. F.; Giltinan, J.; Sitti, M. 3D-printed biodegradable microswimmer for theranostic cargo delivery and release. *ACS Nano* **2019**, *13* (3), 3353−3362.
(26) Zhang, L.; Alimu, G.; Du, Z.; Yan, T.; Li, H.; Ma, R.; Lan, Z.; Yu, Z.; Alifu, N.; Sun, K. Functionalized Magnetic Nanoparticles for NIR-Induced Photothermal Therapy of Potential Application in Cervical Cancer. *ACS Omega* **2023**, *8* (24), 21793−21801.
(27) Sumitha, N. S.; Prakash, P.; Nair, B. N.; Sailaja, G. S. Degradation-dependent controlled delivery of doxorubicin by glyoxal cross-linked magnetic and porous chitosan microspheres. *ACS Omega* **2021**, *6* (33), 21472−21484.
(28) Kandasamy, G.; Sudame, A.; Luthra, T.; Saini, K.; Maity, D. Functionalized hydrophilic superparamagnetic iron oxide nanoparticles for magnetic fluid hyperthermia application in liver cancer treatment. *ACS Omega* **2018**, *3* (4), 3991−4005.
(29) Dogangil, G.; Ergeneman, O.; Abbott, J. J.; Pané, S.; Hall, H.; Muntwyler, S.; Nelson, B. J. Toward targeted retinal drug delivery with wireless magnetic microrobots. *IEEE Int. Conf. Intell. Robots Syst.* **2008**, 1921−1926.
(30) Chatzipirpiridis, G.; Ergeneman, O.; Pokki, J.; Ullrich, F.; Fusco, S.; Ortega, J. A.; Sivaraman, K. M.; Nelson, B. J.; Pané, S. Electroforming of implantable tubular magnetic microrobots for wireless ophthalmologic applications. *Adv. Healthc. Mater.* **2015**, *4* (2), 209−214.
(31) Wu, Z.; Troll, J.; Jeong, H.-H.; Wei, Q.; Stang, M.; Ziemssen, F.; Wang, Z.; Dong, M.; Schnichels, S.; Qiu, T.; Fischer, P. A swarm of slippery micropropellers penetrates the vitreous body of the eye. *Sci. Adv.* **2018**, *4* (11), No. eaat4388.
(32) Yu, J.; Jin, D.; Chan, K.-F.; Wang, Q.; Yuan, K.; Zhang, L. Active generation and magnetic actuation of microrobotic swarms in bio-fluids. *Nat. Commun.* **2019**, *10* (1), 5631.
(33) Kim, D. I.; Lee, H.; Kwon, S. H.; Sung, Y. J.; Song, W. K.; Park, S. Bilayer hydrogel sheet-type intraocular microrobot for drug delivery and magnetic nanoparticles retrieval. *Adv. Healthc. Mater.* **2020**, *9* (13), No. 2000118.
(34) Wang, Y.-F.; Shyu, H.-W.; Chang, Y.-C.; Tseng, W.-C.; Huang, Y.-L.; Lin, K.-H.; Chou, M.-C.; Liu, H.-L.; Chen, C.-Y. Nickel (II)-induced cytotoxicity and apoptosis in human proximal tubule cells through a ROS-and mitochondria-mediated pathway. *Toxicol. Appl. Pharmacol.* **2012**, *259* (2), 177−186.
(35) El-Habit, O. H.; Abdel Moneim, A. E. Testing the genotoxicity, cytotoxicity, and oxidative stress of cadmium and nickel and their additive effect in male mice. *Biol. Trace Elem Res.* **2014**, *159*, 364−372.
(36) Yu, J.; Yang, L.; Zhang, L. Pattern generation and motion control of a vortex-like paramagnetic nanoparticle swarm. *Int. J. Robot. Res.* **2018**, *37* (8), 912−930.
(37) Yu, J.; Jin, D.; Zhang, L. Mobile paramagnetic nanoparticle-based vortex for targeted cargo delivery in fluid. *IEEE int. Conf. Robot. Autom.* 2017; IEEE: pp 6594−6599.
(38) Yu, J.; Zhang, L. Characterising of mobile vortex-like paramagnetic nanoparticle swarm: From a single vortex to multiple vortices. *IEEE Trans Nanotechnol.* 2017; IEEE: pp 293−296.
(39) Kagan, D.; Benchimol, M. J.; Claussen, J. C.; Chuluun-Erdene, E.; Esener, S.; Wang, J. Acoustic droplet vaporization and propulsion of perfluorocarbon-loaded microbullets for targeted tissue penetration and deformation. *Chem. Int. Ed.* **2012**, *51* (30), 7519−7522.
(40) Mou, F.; Chen, C.; Ma, H.; Yin, Y.; Wu, Q.; Guan, J. Self-propelled micromotors driven by the magnesium−water reaction and their hemolytic properties. *Chem. Int. Ed.* **2013**, *52* (28), 7208−7212.
(41) Mou, F.; Chen, C.; Zhong, Q.; Yin, Y.; Ma, H.; Guan, J. Autonomous motion and temperature-controlled drug delivery of Mg/Pt-poly (N-isopropylacrylamide) Janus micromotors driven by simulated body fluid and blood plasma. *ACS Appl. Mater. Interfaces.* **2014**, *6* (12), 9897−9903.
(42) Yi, D. K.; Selvan, S. T.; Lee, S. S.; Papaefthymiou, G. C.; Kundaliya, D.; Ying, J. Y. Silica-coated nanocomposites of magnetic nanoparticles and quantum dots. *J. AM. Chem. Soc.* **2005**, *127* (14), 4990−4991.
(43) Li, C.; Ma, C.; Wang, F.; Xi, Z.; Wang, Z.; Deng, Y.; He, N. Preparation and biomedical applications of core−shell silica/magnetic nanoparticle composites. *J. Nanosci. Nanotechnol.* **2012**, *12* (4), 2964−2972.
(44) Xie, H.; He, Z.; Liu, Y.; Zhao, C.; Guo, B.; Zhu, C.; Xu, J. Efficient antibacterial agent delivery by mesoporous silica aerogel. *ACS Omega.* **2022**, *7* (9), 7638−7647.
(45) Abdelaziz, M. M.; Hefnawy, A.; Anter, A.; Abdellatif, M. M.; Khalil, M. A.; Khalil, I. A. Silica-Coated Magnetic Nanoparticles for Vancomycin Conjugation. *ACS Omega* **2022**, *7* (34), 30161−30170.
(46) Wu, W.; He, Q.; Jiang, C. Magnetic iron oxide nanoparticles: synthesis and surface functionalization strategies. *Nanoscale Res. Lett.* **2008**, *3*, 397−415.
(47) Tamura, H.; Miyamoto, K.; Kiryu, J.; Miyahara, S.; Katsuta, H.; Hirose, F.; Musashi, K.; Yoshimura, N. Intravitreal injection of corticosteroid attenuates leukostasis and vascular leakage in experimental diabetic retina. *Investig. Ophthalmol. Vis. Sci.* **2005**, *46* (4), 1440−1444.
(48) Haller, J. A.; Bandello, F.; Belfort, R., Jr; Blumenkranz, M. S.; Gillies, M.; Heier, J.; Loewenstein, A.; Yoon, Y. H.; Jiao, J.; Li, X.-Y.; Whitcup, S. M.; Ozurdex GENEVA study group. Dexamethasone intravitreal implant in patients with macular edema related to branch or central retinal vein occlusion: twelve-month study results. *Ophthalmology.* **2011**, *118* (12), 2453−2460.
(49) Williams, G. A.; Haller, J. A.; Kuppermann, B. D.; Blumenkranz, M. S.; Weinberg, D. V.; Chou, C.; Whitcup, S. M. Dexamethasone posterior-segment drug delivery system in the treatment of macular edema resulting from uveitis or Irvine-Gass syndrome. *Am. J. Ophthalmol.* **2009**, *147* (6), 1048−1054.
(50) Wang, C.; Hou, H.; Nan, K.; Sailor, M. J.; Freeman, W. R.; Cheng, L. Intravitreal controlled release of dexamethasone from engineered microparticles of porous silicon dioxide. *Exp. Eye Res.* **2014**, *129*, 74−82.
(51) Krishnan, V.; Xu, X.; Barwe, S. P.; Yang, X.; Czymmek, K.; Waldman, S. A.; Mason, R. W.; Jia, X.; Rajasekaran, A. K. Dexamethasone-loaded block copolymer nanoparticles induce leukemia cell death and enhance therapeutic efficacy: a novel application in pediatric nanomedicine. *Mol. Pharmaceutics* **2013**, *10* (6), 2199−2210.

https://doi.org/10.1021/acsomega.3c07033
ACS Omega 2024, 9, 27888−27897

(52) Laane, E.; Tamm, K. P.; Buentke, E.; Ito, K.; Khahariza, P.; Oscarsson, J.; Corcoran, M.; Björklund, A.; Hultenby, K.; Lundin, J.; Heyman, M.; Soderhall, S.; Mazur, J.; Porwit, A.; Pandolfi, P. P.; Zhivotovsky, B.; Panaretakis, T.; Grander, D. Cell death induced by dexamethasone in lymphoid leukemia is mediated through initiation of autophagy. *Cell Death Differ.* **2009**, *16* (7), 1018−1029.
(53) Del Amo, E. M.; Urtti, A. Rabbit as an animal model for intravitreal pharmacokinetics: Clinical predictability and quality of the published data. *Exp. Eye Res.* **2015**, *137*, 111−124.

https://doi.org/10.1021/acsomega.3c07033
ACS Omega 2024, 9, 27888−27897